Experimental Analysis and Design Guidelines for Microphone Virtualization in Automotive Scenarios

Alessandro Opinto, Marco Martalò, Alessandro Costalunga, Nicolò Strozzi, Carlo Tripodi and Riccardo Raheli

***Abstract*—In this paper, a performance analysis on the estimation of the so-called observation filter for the Virtual Microphone Technique (VMT) in a realistic automotive environment is presented. A performance comparison between adaptive and fixed observation filter estimation methods, namely Least Mean Square (LMS) and Minimum Mean Square Error (MMSE), respectively, was carried on. Two different experimental setups were implemented on a popular B-segment car. Eight microphones were placed at the monitoring and virtual positions in order to sense environmental acoustic noise propagating within the cabin of the car running at variable speed on a smooth asphalt. Our experimental results show that a large spectral coherence between monitoring and virtual microphone signals indicates a potentially effective and relatively wide-band virtual microphone signal reconstruction. The fixed observation filter estimation method achieves better performance than the adaptive one, guaranteeing remarkable broadband estimation accuracy. Moreover, for each considered setup, design guidelines are proposed to obtain a good trade-off between estimation accuracy and material costs.**

***Index Terms*—Virtual Microphone Technique, Observation Filter Estimation, Adaptive Filtering, Minimum Mean Square Error, Active Noise Control, Automotive.**

I. INTRODUCTION

THE problem of noise mitigation within the interior of a car cabin is nowadays efficiently overcome thanks to the introduction of acoustic absorbing materials, for medium- and high-frequency audio waves, and employing Active Noise Control (ANC) systems for low-frequency disturbing contributions [1], [2].

Most of the known and commercial ANC solutions create a quite zone around the so-called *error microphone*, whose purpose is to continuously track the temporal evolution of the incoming sound waves in order to attenuate them by proper anti-noise signals. The strategic placement of error microphones plays a key role on sound mitigation performance [3]. In fact, one would ideally achieve noise cancellation in regions as close as possible to driver's or passenger's ears. In the automotive environment, where the positioning of a microphone is usually constrained by the car producer, physically reaching the desired quiet zones may be complicated. Thus, when error microphones can not be placed in particular locations, a Virtual Microphone Technique (VMT) can be employed to ensure effective active noise reduction [4], [5]. The microphone that is aimed to acquire the disturbing signal and to feed it back to the digital signal processor is called *monitoring microphone*, whereas the physical location in which the noise mitigation is desired, e.g., around the driver's or passenger's ears, is referred to as *virtual microphone* [6].

The use of an ANC system with VMT can be considered a valid solution if noise cancellation within the low and medium frequency range is obtained. The idea behind VMT is to retrieve the virtual microphone signals starting from the monitoring ones in order to minimize the disturbing audio waves at the virtual locations [4], [7]. For this reason, the accurate estimation of the acoustic channel between monitoring and virtual microphones, usually called *observation filter*, is necessary [8]–[10]. Several approaches and algorithms were proposed in the literature [11], [12] and efficiently employed in realistic office and automotive scenarios [13]–[15]. Moreover, a valid alternative to the observation filter estimation method (the so-called *additional filter*) was developed in [4], [16], [17].

The aim of this paper is to analyze the observation filter estimation accuracy in a realistic automotive environment and investigate microphone placement for effective signal reconstruction at the virtual position. In particular, two well-known time-domain algorithms, namely the Least Mean Square (LMS) and the Minimum Mean Square Error (MMSE), were employed in order to estimate the observation filter during an offline training period. In both cases, the observation filter is fixed at the end of the training period—in the LMS case, the filter coefficients are freezed at the values reached at the end of training. Related work on the MMSE solution appears in [18]. The LMS method is computationally simpler than the MMSE-based one, which instead may require the inversion of a large matrix. By employing a professional portable multi-track recorder, microphone signals were acquired during experimental measurement campaigns performed in a realistic car interior, i.e., that of a popular B-segment car, at variable paces on smooth asphalt roads. Eight microphones, installed within the car interior, were used in order to record the environmental

This work was supported by ASK Industries S.p.A. and the Italian Ministry of Economic Development (MiSE)'s fund for the sustainable growth (F.C.S.) under grant agreement (CUP) B48I15000130008, project VASM (Vehicle Active Sound Management).

This paper was presented in part at the Int. Conf. on Immersive and 3D Audio (I3DA), Bologna, Italy, September 2021.

A. Opinto is with the Department of Electrical, Electronic, and Information Engineering "Guglielmo Marconi," University of Bologna, Italy and the Department of Engineering and Architecture, University of Parma, Italy, e-mail: alessandro.opinto3@unibo.it.

M. Martalò is with the Department of Electrical and Electronic Engineering, University of Cagliari, Italy and Consorzio Nazionale Interuniversitario per le Telecomunicazioni (CNIT), Italy, e-mail: marco.martalo@unica.it.

A. Costalunga, N. Strozzi and C. Tripodi are with ASK Industries S.p.A., Reggio Emilia, Italy, e-mail: {alessandro.costalunga, nicolo.strozzi, carlo.tripodi}@askgroup.global.

R. Raheli is with the Department of Engineering and Architecture, University of Parma, Italy, and Consorzio Nazionale Interuniversitario per le Telecomunicazioni (CNIT), Italy, e-mail: riccardo.raheli@unipr.it

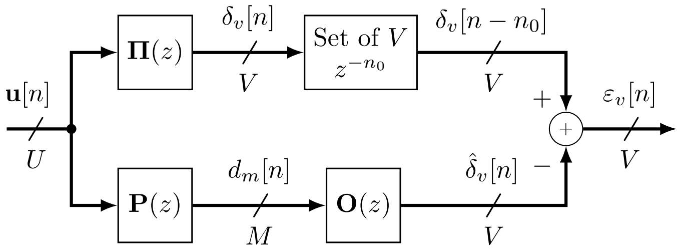

Fig. 1: General block diagram of environmental audio signals propagating within a car cabin, acquired by monitoring and virtual microphones, and their reconstruction by observation filters.

sounds at the monitoring and virtual microphone positions. In fact, during the preparatory tuning period, physical transducers were momentarily placed at the desired virtual locations for observation filter estimation purposes. Despite this approach disregards the potential alteration of the true acoustic channel response caused by the use of physical microphones at the virtual positions, the resulting approximation is considered negligible and acceptable in the literature, see, e.g., [4], [19].

The obtained experimental results on the observation filter estimation are assessed in terms of Mean Square Error (MSE) and Sound Pressure Level (SPL). A performance analysis and comparison among the proposed estimation algorithms is presented. Moreover, for each considered experimental setup, an investigation on the number and location of monitoring microphones needed for improved reconstruction accuracy of the virtual microphone signals is performed. Our analysis provides guidelines on the strategic monitoring microphone placement in order to obtain a significant spectral coherence between monitoring and virtual signals. For both proposed algorithms, the observation filter estimation is remarkably effective at low frequencies. It turns out that the MMSE algorithm achieves better performance than the LMS one, since it exhibits significant and more robust performance also in the medium frequency range, i.e., up to 1000 Hz. This paper expands upon preliminary work appeared in [20], where an initial analysis of adaptive LMS and fixed MMSE algorithms using just one physical microphone was presented for a different automotive scenario.

The rest of this paper is organized as follows. In Section II, the system model is introduced together with the considered experimental setups. The theoretical background on observation filter estimation by means of LMS and MMSE algorithms is reviewed in Section III. Experimental numerical results are presented and discussed in Section IV. Finally, in Section V conclusions are drawn and finale remarks are given.

II. Reference Scenario

A. System Model

A general block diagram for the reconstruction of V virtual microphones by means of M monitoring microphones and VMT with observation filters $\mathbf{O}(z)$ is depicted in Fig. 1, where thick lines represent multiple signals. A set of U unknown environmental audio sources $\mathbf{u}[n]$ propagating within the car interior is detected by the transducers installed at virtual and monitoring positions. The acoustic unknown channels between the disturbing audio sources and the microphones are usually known as *primary paths* and can be modeled by Finite Impulse Response (FIR) filters with transfer functions $\mathbf{P}(z)$ and $\mathbf{\Pi}(z)$. More precisely, at the m-th monitoring microphone, signal $d_m[n]$ is obtained as the product of the m-th row of the matrix filter $\mathbf{P}(z)$ by the input $\mathbf{u}[n]$. Similarly, for the v-th virtual microphone, the corresponding row of the transfer function $\mathbf{\Pi}(z)$ describes the relation between $\mathbf{u}[n]$ and the signal $\delta_v[n]$.

The block $\mathbf{O}(z)$ in Fig. 1 represents the set of VM observation filters. The purpose of these observation filters is to retrieve the set of virtual microphone signals starting from the set of monitoring ones. When main components of the monitoring microphone signals are perceived before the virtual ones, optimal causal observation filters are obtained [9], [15]. However, due to the car interior structure and constraints on the monitoring microphone positioning, environmental audio waves may be first perceived by the virtual microphones and then by the monitoring ones. This implies that a causality condition may not be verified. To deal with this issue, a delay of n_0 samples may be introduced in the sequence of the virtual microphone signals. Thus, at the v-th virtual microphone, the delayed signal $\delta_v[n-n_0]$ is obtained.

From Fig. 1, at the output of block $\mathbf{O}(z)$, the reconstructed version of the v-th virtual microphone signal is obtained, i.e., $\hat{\delta}_v[n]$, and the corresponding error signal can be expressed as

$$\varepsilon_v[n] = \delta_v[n-n_0] - \hat{\delta}_v[n] \ . \tag{1}$$

When a quasi perfect reconstruction of the virtual signal is performed, the error signal $\varepsilon_v[n]$ approaches zero.

B. Experimental Setup

Environmental noise propagating within a car interior was acquired during experimental measurement campaigns performed on a popular B-segment car. Microphone signals were acquired for a duration of about 5 minutes while running the car on roads with smooth asphalt at a variable speed going from 60 km/h (37 mph) to 90 km/h (56 mph). To this end, a well-known professional portable multi-track field recorder with 8 channels was employed. In particular, the first two channels were employed to obtain the audio signals at the virtual microphone positions and the last six channels for the monitoring ones. The acquisition sampling frequency was set to 48 kHz, but in order to reduce the computational complexity, microphone signals were down-sampled from 48 kHz to $f_s = 6$ kHz.

Signal acquisition was performed on a closed path, of length approximately equal to 18 km, moving away and back to the Department of Engineering and Architecture of the University of Parma. The asphalt was approximately smooth during all the trip. On the forward way (approximately 9 km), the weather was cloudy and a truck was ahead of our car. On the return way (approximately 9 km), it started raining and no other cars were close to our. The driving style was approximately uniform during all the acquisition phase (either forward or return), e.g., about the same number of accelerations and decelerations was performed.

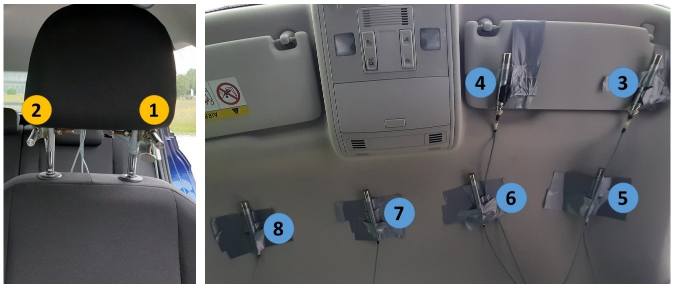

(a) (b)

Fig. 2: Microphone installation within the car interior for the `Roof` setup. Virtual at the driver's headrest (a) and monitoring microphones placement at the driver's sun visor and roof (b).

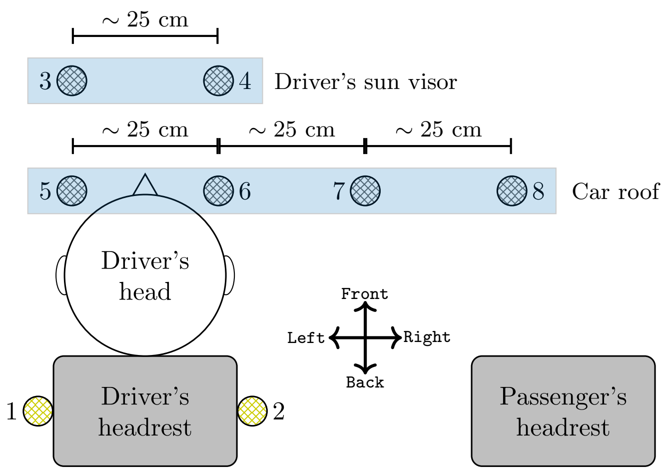

Fig. 3: Representative scheme (top view) of microphones positioning for the `Roof` setup. In yellow and blue, virtual and monitoring microphones, respectively.

(a) (b)

Fig. 4: Microphones installation within car interior for the `Headrest` setup. Virtual at the passenger's ears and monitoring microphones at the sides of the headrest (a). Monitoring microphones positioned around the passenger's headrest perimeter (b).

Based on the monitoring microphone positions, two different experimental setups were considered. In particular, the `Roof` setup is composed of six monitoring microphones, installed at the cabin roof and at the driver's sun visor, and two microphones positioned around the left and right driver's ears for virtual microphone signal acquisition. In Fig. 2, pictures of the microphone installation within the car cabin for the `Roof` setup are shown. Free-field Brüel&Kjær microphones for measurements in transport-noise with a sensitivity of 31.6 mV/Pa were employed. Microphones number 1 and 2, depicted in yellow in Fig. 2 (a), were placed just below the headrest at the maximum possible height in order to acquire virtual microphone signals. In Fig. 2 (b), in blue, microphones number 3, 4, 5, 6, 7 and 8 were used as monitoring ones. More precisely, microphones number 3 and 4 were placed at the left and right side of the driver's sun visor, respectively, whereas microphones number 5, 6, 7 and 8 were positioned at the roof of the car, from left to right, respectively. A representative scheme, with a top view, of microphone positions and corresponding tags is depicted in Fig. 3.

The `Headrest` setup consists of a manikin placed at the front passenger seat equipped with two binaural microphones for recording virtual signals, whereas monitoring ones were obtained by six microphones installed around the headrest perimeter. Pictures for the `Headrest` setup are shown in Fig. 4. A Sennheiser manikin placed at the front passenger seat was equipped with two binaural microphones with a sensitivity of 10 mV/Pa inserted in the manikin's ears in order to collect the perceived virtual microphone signals, as shown in yellow in Fig. 4 (a). Monitoring microphones were symmetrically positioned around the perimeter of the headrest as shown in blue in Fig. 4 (b). In particular, from passenger's left to right, microphones number 3 and 8 were placed at the base of the headrest, microphones number 4 and 7 were positioned at half height of the headrest, as it can be observed in the Fig. 4(a). Finally, microphones number 5 and 6 were installed above the headrest, (see Fig. 4(b)). Note that the employed monitoring microphones are the same as those used in the `Roof` setup. A simplified representation of the considered `Headrest` setup and the corresponding microphone tags is depicted in Fig. 5, (a) front and (b) top view.

These two specific setups were considered since they are representative of main applications of interest. In particular, for the `Roof` setup monitoring microphones were installed at the sun's visor and at the roof to evaluate the effectiveness of an array placed above the head of each car occupant. Such an array can be effectively placed inside the car structure. Similar considerations can be done for the `Headrest` setup, since a microphone array around the head of each occupant can be inserted into the seat headrests.

III. Observation Filter Estimation Algorithms

In this section, the theoretical background on LMS and MMSE observation filter estimation algorithms is reviewed for the case of multiple monitoring and virtual microphones.

A. Adaptive Approach: LMS

The aim of the LMS algorithm is to determine the filter tap-weights which minimize the mean square error. From

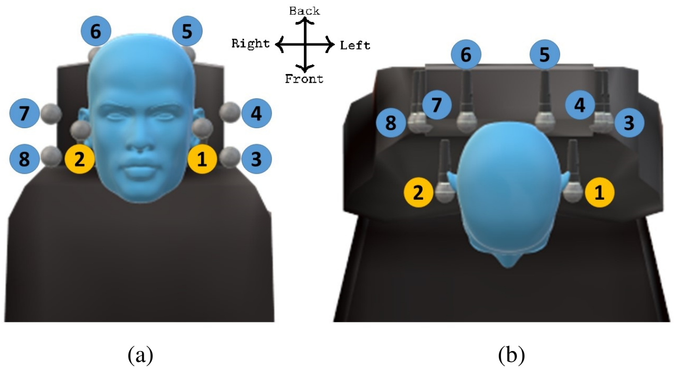

Fig. 5: Representative scheme of microphone positioning for the `Headrest` setup. In yellow and blue virtual and monitoring microphones, respectively. Front view (a), top view (b).

Fig. 1, the v-th reconstructed virtual microphone signal can be expressed as

$$\hat{\delta}_v[n] = \mathbf{o}_v'^{\top}[n]\mathbf{d}'[n] \tag{2}$$

where the MI-length microphone vector is defined as

$$\mathbf{d}'[n] = \left[\mathbf{d}_1^{\top}[n], \mathbf{d}_2^{\top}[n], ..., \mathbf{d}_m^{\top}[n], ..., \mathbf{d}_M^{\top}[n]\right]^{\top} \tag{3}$$

in which $\top$ is the transpose operator, the filter coefficient vector is defined as

$$\mathbf{o}_v'[n] = \left[\mathbf{o}_{v1}^{\top}[n], \mathbf{o}_{v2}^{\top}[n], ..., \mathbf{o}_{vm}^{\top}[n], ..., \mathbf{o}_{vM}^{\top}\right]^{\top} \tag{4}$$

and for the m-th monitoring microphone, vectors in (3) and (4) are respectively defined as

$$\mathbf{d}_m[n] = [d_m[n], d_m[n-1], ..., d_m[n-I+1]]^{\top} \tag{5}$$

$$\mathbf{o}_{vm}[n] = [o_{vm0}[n], o_{vm1}[n], ..., o_{vm,I-1}[n]]^{\top} \tag{6}$$

where I is the observation filter length. The vector in (6) denotes the impulse response at the n-th time epoch of the adaptive filter from the v-th virtual microphone signal to the m-th monitoring one.

The tap-weight update equation of the leaky normalized LMS algorithm for the observation filter between the m-th monitoring and the v-th virtual microphone at the n-th time epoch is [21]

$$\mathbf{o}_{vm}[n+1] = \lambda\mathbf{o}_{vm}[n] + \mu\varepsilon_v[n]\frac{\mathbf{d}_m[n]}{\alpha + \mathbf{d}_m^{\top}[n]\mathbf{d}_m[n]} \tag{7}$$

where the *step-size parameter* μ controls the algorithm convergence speed, $\lambda \in [0,1]$ is the so-called *leakage factor* which sets the algorithm memory and α is a positive constant introduced in order to prevent computational errors when the normalization factor $\mathbf{d}_m^{\top}[n]\mathbf{d}_m[n]$ is too small.

B. Fixed Approach: MMSE

Similarly to (2), at the output of the observation filter, the retrieved signal of the v-th virtual microphone can be expressed as

$$\hat{\delta}_v[n] = \mathbf{d}'^{\top}[n]\mathbf{o}_v' = \mathbf{o}_v'^{\top}\mathbf{d}'[n] \tag{8}$$

having previously defined these vectors in (3) and (4). Note that, since the tap-weights are now time independent, in (8), the index n has been dropped.

The Mean Square Error (MSE) of $\varepsilon_v[n]$, can now be expressed as

$$\begin{aligned}\mathbb{E}\left\{\varepsilon_v[n]\varepsilon_v^{\top}[n]\right\} &= \mathbb{E}\left\{\left(\delta_v[n-n_0] - \hat{\delta}_v[n]\right)^2\right\} \\ &= c_{\delta_v} - 2\mathbf{c}_{\mathbf{d}'\delta_v}^{\top}\mathbf{o}_v' + \mathbf{o}_v'^{\top}\mathbf{C}_{\mathbf{d}'\mathbf{d}'}\mathbf{o}_v'\end{aligned} \tag{9}$$

where $\mathbb{E}\{\cdot\}$ denotes the expectation operator, $c_{\delta_v} = \mathbb{E}\left\{\delta_v^2[n-n_0]\right\}$ is the mean square value of the v-th virtual microphone signal, $\mathbf{c}_{\mathbf{d}'\delta_v} = \mathbb{E}\left\{\mathbf{d}'[n]\delta_v[n-n_0]\right\}$ is the cross-correlation vector between the monitoring microphone vector and the v-th virtual microphone signal and $\mathbf{C}_{\mathbf{d}'\mathbf{d}'} = \mathbb{E}\left\{\mathbf{d}'[n]\mathbf{d}'^{\top}[n]\right\}$ denotes the auto-correlation matrix of the monitoring microphone vector. Thus, by minimizing (9) with respect to the v-th observation filter tap weights, the resulting optimal impulse response becomes

$$\mathbf{o}_v' = \left[\mathbf{C}_{\mathbf{d}'\mathbf{d}'} + \beta\mathbf{I}_{MI}\right]^{-1}\mathbf{c}_{\mathbf{d}'\delta_v} \tag{10}$$

where β is a regularization factor introduced since the auto-correlation matrix may be ill-conditioned [9], [22] and $\mathbf{I}_{MI}$ denotes the identity matrix of size $MI \times MI$.

The cross-correlation vector $\mathbf{c}_{\mathbf{d}'\delta_v}$ can be expressed as

$$\begin{aligned}\mathbf{c}_{\mathbf{d}'\delta_v} &= \mathbb{E}\left\{\begin{bmatrix}\mathbf{d}_1[n] \\ \mathbf{d}_2[n] \\ \vdots \\ \mathbf{d}_M[n]\end{bmatrix}\delta_v[n-n_0]\right\} \\ &= [g_{v1}[0], ..., g_{v1}[I-1], ..., g_{vM}[0], ..., g_{vM}[I-1]]^{\top}\end{aligned} \tag{11}$$

where the element $g_{vm}[t]$ can be estimated as a temporal correlation on a window of length $N_1 - N_0$, i.e.,

$$\begin{aligned}g_{vm}[t] &= \mathbb{E}\left\{d_m[n-t]\delta_v[n-n_0]\right\} \\ &\simeq \frac{1}{N_1 - N_0}\sum_{n=N_0}^{N_1-1} d_m[n-t]\delta_v[n-n_0]\end{aligned} \tag{12}$$

where $0 \leq t \leq I-1 \leq N_0$ for $v = 1, 2, ..., V$ and $m = 1, 2, .., M$. The auto-correlation matrix $\mathbf{C}_{\mathbf{d}'\mathbf{d}'}$ defined as

$$\begin{aligned}\mathbf{C}_{\mathbf{d}'\mathbf{d}'} &= \mathbb{E}\left\{\mathbf{d}'[n]\mathbf{d}'^{\top}[n]\right\} \\ &= \mathbf{E}\left\{\begin{bmatrix}\mathbf{d}_1[n]\mathbf{d}_1^{\top}[n] & \cdots & \mathbf{d}_1[n]\mathbf{d}_M^{\top}[n] \\ \vdots & \ddots & \vdots \\ \mathbf{d}_M[n]\mathbf{d}_1^{\top}[n] & \cdots & \mathbf{d}_M[n]\mathbf{d}_M^{\top}[n]\end{bmatrix}\right\}\end{aligned} \tag{13}$$

can also be formulated in terms of the square matrices of size $I \times I$

$$\begin{aligned}\mathbf{R}_{\ell k} &= \mathbb{E}\left\{\mathbf{d}_\ell[n]\mathbf{d}_k^{\top}[n]\right\} \\ &= \begin{bmatrix} r_{lk}[0] & r_{lk}[1] & \cdots & r_{lk}[I-1] \\ r_{lk}[-1] & r_{lk}[0] & \cdots & r_{lk}[I-2] \\ \vdots & \vdots & \ddots & \vdots \\ r_{lk}[-I+1] & r_{lk}[-I+2] & \cdots & r_{lk}[0]\end{bmatrix}.\end{aligned} \tag{14}$$

Similarly to (12), the element $r_{\ell k}[t]$ of (14) can be estimated as a temporal correlation, i.e.,

$$\begin{aligned} r_{\ell k}[t] &= \mathbb{E}\left\{d_\ell[n]d_k[n-t]\right\} \\ &\simeq \frac{1}{N_1-N_0}\sum_{n=N_0}^{N_1-1} d_\ell[n]d_k[n-t] \end{aligned} \tag{15}$$

with $0 \leq t \leq I-1 \leq N_0$ for $r, l = 1, 2, ..., M$. Assuming cross stationarity of the signals $d_k[n]$ and $d_\ell[n]$, the following symmetry property arises

$$\begin{aligned} r_{k\ell}[t] &= \mathbb{E}\left\{d_k[n]d_\ell[n-t]\right\} \\ &= \mathbb{E}\left\{d_\ell[n]d_k[n+t]\right\} \\ &= r_{\ell k}[-t]\ . \end{aligned} \tag{16}$$

Hence, the matrix $\mathbf{R}_{\ell k}$ defined in (14) can also be expressed as

$$\mathbf{R}_{\ell k} = \begin{bmatrix} r_{\ell k}[0] & r_{\ell k}[1] & \cdots & r_{\ell k}[I-1] \\ r_{k\ell}[1] & r_{\ell k}[0] & \cdots & r_{\ell k}[I-1] \\ \vdots & \vdots & \ddots & \vdots \\ r_{k\ell}[I-1] & r_{k\ell}[I-2] & \cdots & r_{\ell k}[0] \end{bmatrix}. \tag{17}$$

Finally, by exploiting the property in (16) and collecting the definitions in (17) and (13), the auto-correlation matrix $\mathbf{C}_{\mathbf{d}'\mathbf{d}'}$ can be written as

$$\begin{aligned} \mathbf{C}_{\mathbf{d}'\mathbf{d}'} &= \begin{bmatrix} \mathbf{R}_{11} & \mathbf{R}_{12} & \cdots & \mathbf{R}_{1M} \\ \mathbf{R}_{21} & \mathbf{R}_{22} & \cdots & \mathbf{R}_{2M} \\ \vdots & \vdots & \ddots & \vdots \\ \mathbf{R}_{M1} & \mathbf{R}_{M2} & \cdots & \mathbf{R}_{MM} \end{bmatrix} \\ &= \begin{bmatrix} \mathbf{R}_{11} & \mathbf{R}_{12} & \cdots & \mathbf{R}_{1M} \\ \mathbf{R}_{12}^\top & \mathbf{R}_{22} & \cdots & \mathbf{R}_{2M} \\ \vdots & \vdots & \ddots & \vdots \\ \mathbf{R}_{1M}^\top & \mathbf{R}_{2M}^\top & \cdots & \mathbf{R}_{MM} \end{bmatrix}. \end{aligned} \tag{18}$$

IV. Experimental Results

In this section, experimental results on observation filter estimation, both for adaptive and fixed approaches, are presented.

50% of the microphone signal acquisition time is spent for observation filter estimation according to the adopted algorithm as described in Section III (training period). Once the impulse responses are obtained, they are tested within the remaining 50% of the same microphone measurement (validation period). In particular, we consider the first half of the return path for training and the last half for validation.

With both filter estimation methods (LMS or MMSE) the algorithm is run in an offline training period (corresponding to half of the simulation time). In the LMS algorithm, the filter coefficients are adapted during this period. At the end of this training period, the filter coefficients are freezed and then used (as time-invariant) in the following validation period (corresponding to the normal system operational condition). The convergence of the LMS algorithm is obviously a crucial aspect in determining the filter coefficients. Similarly, the MMSE algorithm is run using the audio signals acquired during the training period and the obtained (fixed) filter coefficients are then used in the following validation period.

The accuracy of the observation filter estimate is assessed in terms of MSE normalized with respect to the mean square value of the input signal within the validation period. For the v-th virtual microphone this normalized MSE, in logarithmic scale, is defined as

$$\Upsilon_v = 10\log_{10}\frac{\sum_{n=n_0}^{N-1}\varepsilon_v^2[n]}{\sum_{n=n_0}^{N-1}\delta_v^2[n-n_0]} \quad \text{[dB]} \tag{19}$$

where N specifies the time window length of $N-n_0$ samples for MSE evaluation. Ideally, when a perfect reconstruction of the v-th virtual microphone signal is obtained, $\varepsilon_v[n] \to 0$ and $\Upsilon_v \to -\infty$. In particular, to have an efficient performance indicator over the whole frequency band, the MSE is evaluated for 1- and 1/3-octave bands, i.e., error and input signal in (19) are decomposed into octave and fractional-octave subbands [23], [24].

The observation filter length I and the delay n_0 introduced in the virtual microphone sequence are empirically chosen in order to maximize, per each scenario, the MSE performance. Similarly, the step-size parameter μ, leakage factor λ in (7), and regularization factor β in (10) are experimentally set. In particular, in our simulations the step-size is $\mu = 10^{-3}$, no leakage factor is employed, i.e., $\lambda = 1$, and the regularization factor is $\beta = 10^{-6}$.

A necessary condition to obtain good observation filter performance is a sufficiently high correlation between monitoring and virtual microphone signals—in fact, the higher the correlation among such signals, the easier the observation filter estimation. Therefore, a spectral coherence analysis can be pursued in order to investigate the physical limitations of the considered experimental setup. For the v-th virtual microphone signal $\delta_v[n]$ and a matrix of monitoring microphone signals $\mathbf{D} = [\mathbf{d}_1[n], \mathbf{d}_2[n], \ldots, \mathbf{d}_M[n]]^\top$, the multiple spectral coherence $C_{\mathbf{D},\delta_v}(f)$ is defined as [25]

$$C_{\mathbf{D},\delta_v}(f) = \frac{P^\dagger_{\mathbf{D},\delta_v}(f)P^{-1}_{\mathbf{D},\mathbf{D}}(f)P_{\mathbf{D},\delta_v}(f)}{P_{\delta_v\delta_v}(f)} \tag{20}$$

where $P_{\mathbf{D},\mathbf{D}}(f)$ and $P_{\delta_v\delta_v}(f)$ denote the self and cross power spectral densities of monitoring and virtual microphone signals, respectively, $P_{\mathbf{D},\delta_v}(f)$ represents their cross power spectral density and $\dagger$ indicates the Hermitian operator. Since $C_{\mathbf{D},\delta_v}(f) \in [0,1]$, for $C_{\mathbf{D},\delta_v}(f) \simeq 1$, the signals are highly correlated; on the other hand for $C_{\mathbf{D},\delta_v}(f) \simeq 0$, the signals are uncorrelated.[1]

Finally, the SPL spectrum measures the sound pressure of an acoustic wave with respect to a reference sound source. In logarithmic scale it is defined as

$$S(f) = 20\log_{10}\left(\frac{p(f)}{p_0}\right) \quad \text{[dB]} \tag{21}$$

where $p(f)$ is the sound pressure with a frequency resolution that in our simulations is set to about 0.75 Hz, centered at frequency f, and $p_0 = 20\ \mu$Pa is the reference sound pressure.

[1] During the review process, a recent similar analysis was brought to our attention [26].

TABLE I: Summary on the considered scenarios in experimental `Roof` setup. The employed parameters for LMS and MMSE algorithms are also shown.

SCENARIO	M	MICROPHONE TAG	LMS		MMSE	
			n_0	I	n_0	I
A	2	3,4	175	750	200	750
B		5,6	100	500	75	500
C	4	3,4,5,6	100	500	200	1500
D		5,6,7,8	100	500	200	1500
E	6	3, 4, 5, 6, 7, 8	200	500	200	1500

Moreover, in order to take into account the sensitivity of the human ear, an A-weighting filter is applied to the microphone signals [27]. Thus, the SPL spectrum unit measure is expressed in dBA/Hz.

Numerical results are organized based on the monitoring microphone positioning, i.e., `Roof` and `Headrest` setups. In particular, for lack of space, only the left and right virtual positions are here discussed for `Roof` and `Headrest` setups, respectively. These positions, in fact, represent the most relevant ones, since the main noise components within the car cabin is the wind noise from the window (left and right side of the `Roof` and `Headrest` setup, respectively). Note that, for each setup, similar conclusions can be drawn for both virtual microphones.

A. *`Roof` Setup*

In this section, a performance comparison between the LMS and MMSE algorithms for the `Roof` setup is presented. In order to identify the optimal monitoring microphone positioning that optimizes the performance in terms of virtual signal reconstruction accuracy, five different scenarios were considered. Table I summarizes the considered scenarios (see also Figs. 2 and 3).

For each scenario, the spectral coherence between monitoring and left virtual microphone signals is shown in Fig. 6. Note that, for the sake of clarity and VMT physical operating limits, only the interval from 0 to 1000 Hz is depicted. For all the considered scenarios, it is possible to observe that a significant coherence, up to 400 Hz, is exhibited. Except for some specific peaks, e.g., one about 750 Hz, the coherence degrades with increasing frequency. Moreover, by comparing each specific scenario for a fixed number of monitoring microphones, it is possible to conclude that, the choice of placing monitoring transducers at the roof, i.e., microphones number 5 and 6 (Scenario B), is potentially more effective than positioning them at the driver's sun visor, i.e., microphones number 3 and 4 (Scenario A). This is due to the reduced distance between virtual and monitoring microphones. Similarly, by considering four monitoring microphones, Scenario C exhibits better coherence than Scenario D. Finally, the use of all six available monitoring microphones, i.e., Scenario E, shows the highest coherence. This is expected, since the spectral coherence is non-negative by definition and adding information, i.e., more physical microphones, cannot reduce it.

As a preliminary performance investigation, we analyze the convergence of the LMS algorithm in an illustrative example employing the `Roof` setup in scenario E, with 6 physical microphones virtualizing the left error microphone. The obtained results are presented in Fig. 7, where the sliding window SPL (in dB) is shown as a function of time for the considered scenario and various values of the step-size parameter μ. The end time of the training period $t = T_{\text{adapt}}^{\text{stop}}$ is highlighted. The sliding window SPL is defined as

$$L_\varepsilon[n] = 10 \log_{10} \frac{\sum_{\ell=0}^{Q-1} \varepsilon_v^2[n-\ell]}{\sum_{\ell=0}^{Q-1} \delta_v^2[n-n_0-\ell]} \tag{22}$$

where $Q = f_s = 6000$ samples (i.e., one second of audio signals) is the used window length. Note that this quantity is normalized to the input signal energy. It is possible to observe that, during the training period, the higher the step-size the

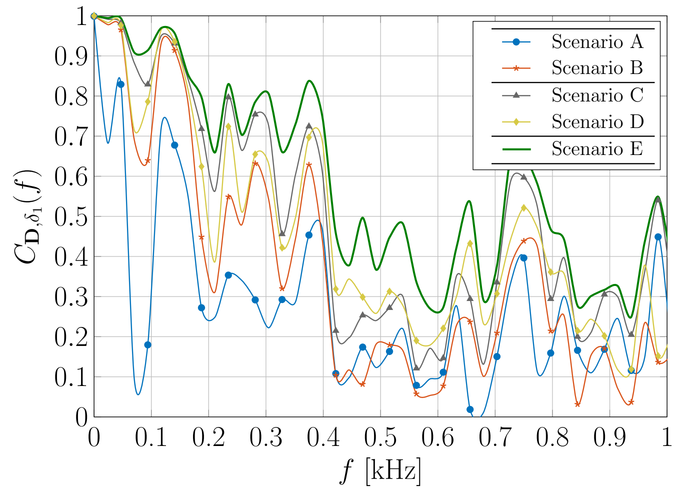

Fig. 6: Spectral coherence per scenario for the `Roof` setup between monitoring microphone signals and the left virtual one.

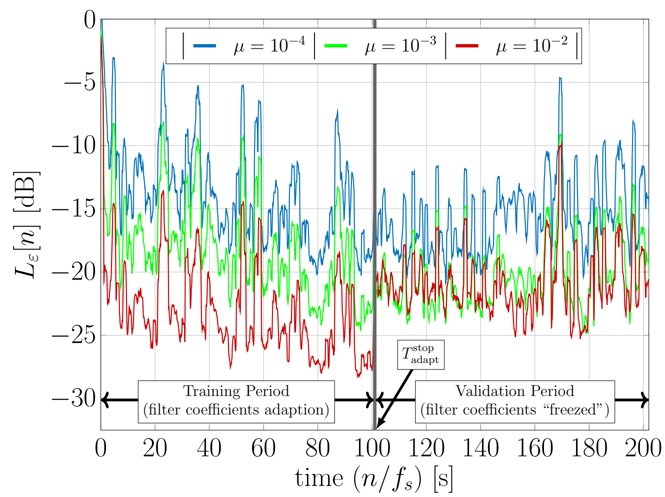

Fig. 7: Sliding window SPL, as a function of time, for an illustrative example employing the `Roof` setup in scenario E with 6 physical microphones virtualizing the left error microphone.

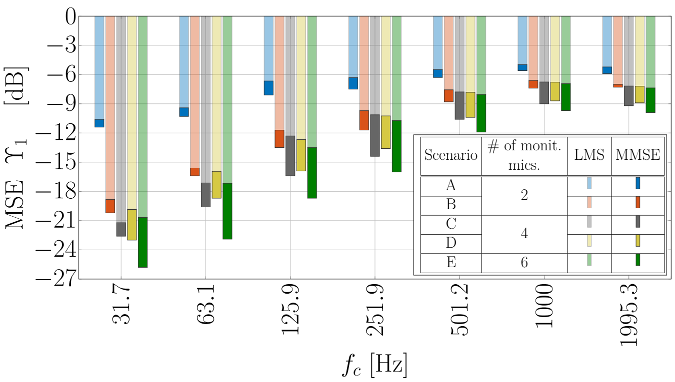

Fig. 8: Performance comparison in terms of normalized MSE as a function of 1-octave band, between adaptive (LMS) and fixed (MMSE) observation filter estimation, at the left virtual microphone position for all the considered scenarios in the `Roof` setup.

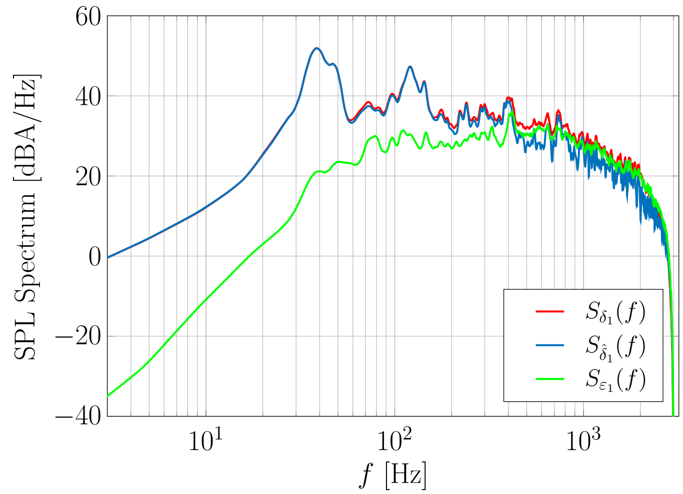

Fig. 9: SPL spectra of left virtual microphone signal (red), its reconstructed version (blue) by means of six monitoring microphones (Scenario E) with the MMSE algorithm and the corresponding error signal (green) for the `Roof` setup.

better the system performance. This is expected, since the LMS algorithm is able to more easily track the rapid oscillation of the time-varying input signal statistics, provided the step size is not too large to prevent instability. On the other hand, during the validation period, if the step-size is high, e.g., 10^{-2}, the performance degrades since the obtained freezed filter coefficients at time $t = T_{\text{adapt}}^{\text{stop}}$ do not precisely identify the correct observation filter. Therefore, we heuristically choose an intermediate step-size with good performance in the validation period, so that the filter coefficients can represent an average signal behavior that can be easily tracked.

In the following, we compare the performance achieved by the adaptive LMS and fixed MMSE filter estimation approaches by considering the optimal cases, i.e., the cases with the minimum possible MSE. To this end, we try various values of n_0 and I; the optimal values are listed in Table I.

MSE performance comparison between LMS (semi-transparent bars) and MMSE (solid bars) estimation algorithms for the reconstruction of the left virtual microphone signal is shown in Fig. 8. In particular, the normalized MSE is shown as a function of 1-octave frequency bands, where f_c denotes the center frequency of the employed second-order sub-band filters and the MSE values are obtained with a value of N in (19) corresponding to the full duration of the validation period. By comparing these approaches, it is possible to observe that the fixed one performs better than the adaptive one, regardless of the considered scenario. As expected, good performance is obtained for the low-frequency regime, i.e., within 0–500 Hz, whereas MSE deteriorates when the frequency increases. By fixing the number of employed monitoring microphones, it is worth noting that Scenario B performs better than Scenario A. This demonstrates that, in order to virtualize signals at the driver position, the placement of two monitoring microphones at the roof is preferable with respect to positioning them at the driver's sun visor. When four monitoring microphones are employed to reconstruct the left virtual microphone, Scenario C performs slightly better than D. Finally, by considering the MMSE algorithm, it is possible to conclude that if six monitoring microphones are available (Scenario E), in the low-frequency range, up to 3.3 dB and 6.5 dB are gained with respect to the case of using four and two monitoring microphones, respectively.

For MMSE observation filter estimation with six monitoring microphones (Scenario E), the SPL spectra of left virtual microphone signal $\delta_1[n]$, its estimated version $\hat{\delta}_1[n]$ and the corresponding error signal $\varepsilon_1[n]$ are shown in Fig. 9. As previously mentioned, it is possible to note that the main energy contribution of the noise propagating within the car interior is concentrated in the low-frequency regime, i.e., 0–500 Hz. Main peak power contributions are present at about 35 Hz, 120 Hz and 240 Hz. The first peak level may be likely due to the first harmonic of the engine, whereas the last one may be caused by the cavity modes of a rolling tire [28], [29]. One can notice that up to 300 Hz, a good reconstruction of the left virtual microphone signal is obtained, since the green curve is below the red one, representing the target signal, by several dBs. The virtual signal reconstruction accuracy decreases with the frequency. In fact, it is possible to note that, above 500 Hz, the observation filter is less effective, since the reconstructed signal does not approach the target one, causing thus a degradation of the system performance. Similar behaviors were observed for other scenarios and microphone setups.

Finally, the observation filter estimation robustness against a mismatch in the operational environment is analyzed. In fact, one would desire that the filter coefficients, computed using the audio signal recorded under a specific scenario (e.g., type of road, vehicle speed, etc.), would be effective also under slightly different conditions. Therefore, we perform a robustness test in which the observation filter is estimated in a particular driving scenario, but then employed in a different one. In particular, we consider the signals acquired in the forward path for training (with cloudy, but not raining weather), whereas the first half of the return path is considered

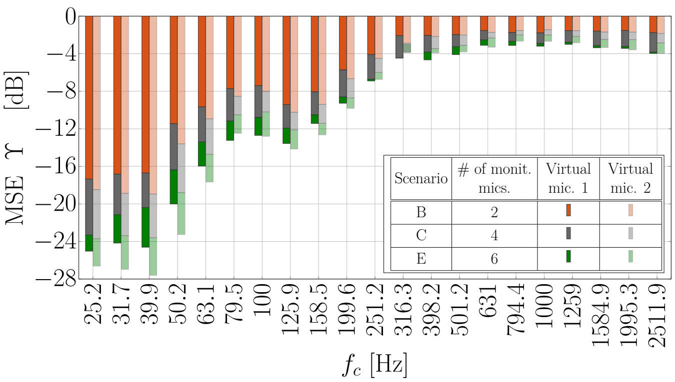

Fig. 10: Performance comparison in terms of normalized MSE measured over the entire duration of recorded signals as a function of 1/3-octave bands with MMSE observation filter estimation in case of road mismatch and the `Roof` setup.

TABLE II: Summary on the considered scenarios in experimental `Headrest` setup. The employed parameters for LMS and MMSE algorithms are also shown.

Scenario	M	Microphone Tag	LMS		MMSE	
			n_0	I	n_0	I
A	2	3,8	150	500	75	1000
B		4,7	150	500	75	750
C		5,6	125	500	200	1000
D	4	3,4,7,8	150	500	75	750
E		4,5,6,7	125	500	75	750
F	6	3, 4, 5, 6, 7, 8	150	500	75	750

for validation (with raining conditions). Numerical results, assessed in terms of normalized MSE against 1/3-octave bands, for Scenarios B, C and E, are shown in Fig. 10 for both virtual microphone signals with MMSE observation filter estimation. This analysis confirms, as previously noticed, that the estimation accuracy improves with increasing number of monitoring microphones and the right virtual microphone performance is slightly improved with respect to the left one for all the considered frequency bands. This difference between left and right virtual positions, may be due to the fact that, since one of the most important noise components within car cabin is given by the wind noise generated from the window (left hand-side of the driver), the signal at the driver's right ear is less noisy than the left one, facilitating thus, the observation filter estimation task. In general, it is possible to conclude that, for both virtual microphones, significant robustness under road mismatch is obtained.

B. `Headrest` Setup

Similarly to the previous setup, for the `Headrest` setup, six scenarios are considered in order to find the best monitoring microphone positioning on the headrest. Table II summarizes the analyzed scenarios and microphone tags (see also Figs. 4 and 5). The spectral coherence per scenario for the right virtual microphone is depicted in Fig. 11. Thanks to the reduced distance between monitoring and virtual microphones, potentially increased performance with respect to the

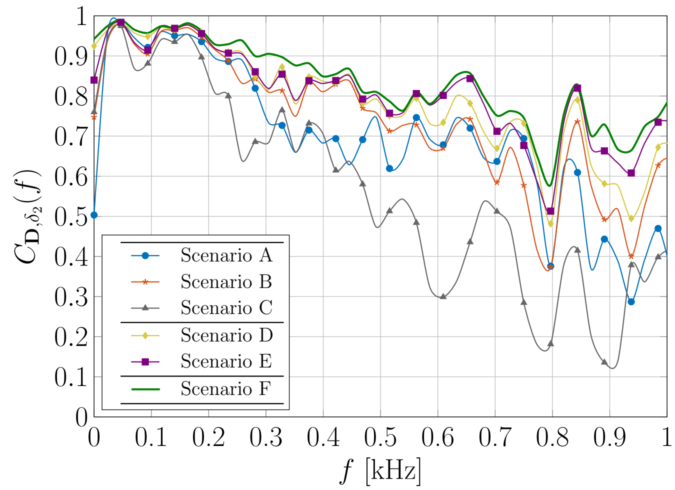

Fig. 11: Spectral coherence per scenario for the `Headrest` setup between monitoring microphone signals and the right virtual one.

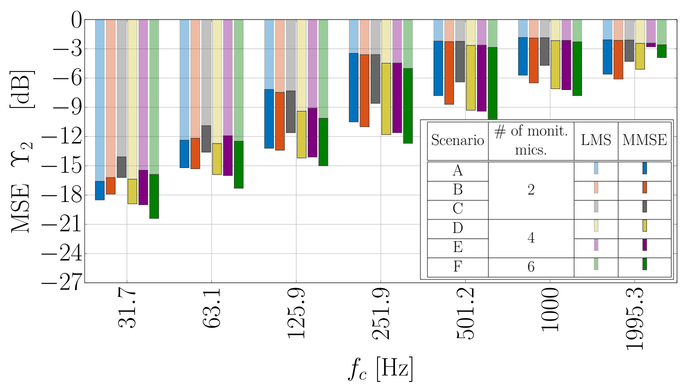

Fig. 12: Performance comparison in terms of normalized MSE as a function of octave band between adaptive (LMS) and fixed (MMSE) observation filter estimation approaches at the right virtual microphone position for all the considered scenarios in the `Headrest` setup.

`Roof` setup is shown, since significant coherence level, up to 1000 Hz, is exhibited when six monitoring microphones are employed. It is possible to observe that Scenarios A and B show better coherence than Scenario C. Scenario B, in fact, shows best coherence when two monitoring microphones are used. Scenario E displays slightly better coherence than D. Finally, best coherence is exhibited by Scenario F.

Performance comparison, in terms of normalized MSE against octave bands, between LMS and MMSE observation filter estimation algorithms, for the right virtual microphone, is depicted in Fig. 12. As in Table I, optimal values of n_0 and I are listed in Table II. Similarly to what already observed in Section IV-A, the MSE degrades for increasing frequency. However, significant wide-band performance is exhibited by the MMSE approach with respect to the LMS one, since an almost double dB improvement in MSE is shown, e.g., for Scenario F at 1000 Hz. The MMSE algorithm confirms once again itself as the best observation filter estimation approach.

By comparing these scenarios under the same number of monitoring microphones, it is possible to confirm what predicted in the previous spectral coherence analysis. In fact, Scenario B, i.e., microphones number 4 and 7, performs better than the Scenarios A and C. This suggests that if two monitoring microphones at the headrest are used, best performance is obtained when they are placed at half height of the headrest. In the low-frequency regime, significant improvement is exhibited thanks the use of four monitoring microphones (Scenario E). This gain with respect to Scenario B reduces when the frequency increases. Finally, the observation that the higher the number of monitoring microphones, the better the performance, remains valid in this case also, since MSE performance is maximized for Scenario F.

Finally, even if a direct comparison between `Roof` and `Headrest` setups cannot be pursued, due to the differences in the microphone installation and virtualization positions, it is expected that the observation filter performs well in a wider-band when the monitoring microphones are positioned at the headrest, since it is effective almost up to 1000 Hz. In fact, both scenarios are analyzed under worst-case conditions, where the virtualization point is closer to the car window, which is a source of strong and undesired signal reflections as well as noise.

V. Concluding Remarks

In this paper, we present an analysis on the accuracy of the observation filter estimation for VMT in a realistic automotive scenario. Based on the monitoring microphone positioning, two experimental setups, consisting of a total of six monitoring microphones, namely `Roof` and `Headrest` setups, are implemented in a popular B-segment car. Similarly, two virtual microphones are placed near the driver's and passenger's ears. Microphone signal acquisitions are performed during experimental measurement campaigns while the car runs at variable speeds on a smooth asphalt.

For the observation filter estimation, two algorithms, namely LMS and MMSE, are employed and compared in order to find the approach which guarantees good performance in terms of virtual microphone signal reconstruction. In order to have a preliminary estimate of the observation filter potential performance, for each considered setup and for different scenarios, a spectral coherence analysis between monitoring and virtual microphones is performed.

Our experimental results show that the MMSE algorithm may represent a valid solution, since it ensures remarkably robust performance in the low-frequency regime, but also appreciable one at higher frequencies. Moreover, pragmatic and heuristic guidelines on positioning and number of monitoring microphones to effectively virtualize specific positions are suggested.

References

[1] P. N. Samarasinghe, W. Zhang and T. D. Abhayapala, "Recent advances in active noise control inside automobile cabins: Toward quieter cars," *IEEE Sign. Proc. Mag.*, vol. 33, no. 6, pp. 61–73, 2016.

[2] S. J. Elliott, P. Nelson, A. M. McDonald, D. C. Quinn, and T. Saunders, "The active control of engine noise inside cars," *In Proceedings of the INTER-NOISE*, pp. 987–990, Sep. 1988.

[3] S. M. Kuo and D. Morgan, "Active noise control: a tutorial review," *Proceedings of the IEEE*, vol. 87, no. 6, pp. 943–973, 1999.

[4] M. Pawelczyk, "Adaptive Noise Control Algorithms for Active Headrest System," *Control Engineering Practice*, vol. 12, pp. 1101–1112, 2004.

[5] B. S. Cazzolato, "An adaptive LMS virtual microphone," *in Proc. Active*, pp. 105–116, January 2002.

[6] D. Moreau, B. Cazzolato, A. Zander, and C. Petersen, "A review of virtual sensing algorithms for active noise control," *Algorithms*, vol. 1, no. 2, pp. 69–99, 2008.

[7] J. Garcia-Bonito, S. J. Elliott and C. C. Boucher, "Generation of zones of quiet using a virtual microphone arrangement," *J. Acoust. Soc. Am.*, vol. 101, no. 6, pp. 3498–3516, 1997.

[8] S. J. Elliott and J. Cheer, "Modeling local active sound control with remote sensors in spatially random pressure fields," *The Journal of the Acoustical Society of America*, vol. 137, no. 4, pp. 1936–1946, 2015.

[9] W. Jung, S. J. Elliott, and J. Cheer, "Local active control of road noise inside a vehicle," *Mechanical Systems and Signal Processing*, vol. 121, pp. 144–157, 2019.

[10] S. Elliott, W. Jung, and J. Cheer, "Causality and robustness in the remote sensing of acoustic pressure, with application to local active sound control," in *ICASSP 2019 - 2019 IEEE International Conference on Acoustics, Speech and Signal Processing (ICASSP)*, 2019, pp. 8484–8488.

[11] C. D. Peterson, R. Fraanje, B. S. Cazzolato, A.C. Zander and C. H. Hansen, "A Kalman filter approach to virtual sensing for active noise control," *Mech. Syst. Signal Process.*, vol. 22, no. 2, pp. 490–508, 2008.

[12] D. J. Moreau, J. Ghan, B. S. Cazzolato, and A. C. Zander, "Active noise control in a pure tone diffuse sound field using virtual sensing," in *The Journal of the Acoustical Society of America*, vol. 125, no. 6, 2009, pp. 3742–3755.

[13] W. Jung, S. J. Elliott, and J. Cheer, "Estimation of the pressure at a listener's ears in an active headrest system using the remote microphone technique," *The Journal of the Acoustical Society of America*, vol. 143, no. 5, pp. 2858–2869, 2018.

[14] D. Das, D. Moreau, and B. Cazzolato, "Performance evaluation of an active headrest using the remote microphone technique," *in Proc. Australian Acoustical Society Conference, Acoustics 2011: Breaking New Ground*, pp. 1–7, November 2011.

[15] S. Elliott, C. K. Lai, T. Vergez, and J. Cheer, "Robust stability and performance of local active control systems using virtual sensing," *in Proc. 23rd. Intern. Congress on Acoustics 2019*, pp. 61–68.

[16] D. Shi, B. Lam, and W.-s. Gan, "Analysis of multichannel virtual sensing active noise control to overcome spatial correlation and causality constraints," in *in Proc. IEEE Intern. Conference on Acoustics, Speech and Signal Processing (ICASSP 2019)*, 2019, pp. 8499–8503.

[17] J. Zhang, S. J. Elliott, and J. Cheer, "Robust performance of virtual sensing methods for active noise control," *Mechanical Systems and Signal Processing*, vol. 152, p. 107453, 2021.

[18] S. J. Elliott and J. Cheer, "Modeling local active sound control with remote sensors in spatially random pressure fields." *The Journal of the Acoustical Society of America*, vol. 137, no. 4, p. 1936–1946, Apr. 2015.

[19] M. Pawelczyk, "Control algorithms for colating zones of quiet in the active headrest system," *Molecular and Quantum Acoustics*, vol. 23, pp. 339–350, 2002.

[20] A. Opinto, M. Martalò, A. Costalunga, N. Strozzi, C. Tripodi and R. Raheli, "Experimental Results on Observation Filter Estimation for Microphone Virtualization," *in Proc. Intern. Conference on Immersive and 3D Audio*, pp. 1–7, September 2021.

[21] M. H. Hayes, *Statistical Digital Signal Processing and Modeling*, 1 ed. New York, NY, USA: John Wiley & Sons, 1996.

[22] F. M. Fazi and P. Nelson, "The ill-conditioning problem in sound field reconstruction," *Journal of the Audio Engineering Society*, October 2007.

[23] "American National Standard Specification for Octave-Band and Fractional-Octave-Band Analog and Digital Filters," Acoustical Society of America, Melville, NY, Standard, 2009.

[24] S. J. Orfanidis, *Introduction to Signal Processing*. Englewood Cliffs, NJ: Prentice Hall, 2010.

[25] S. Kay, *Modern Spectral Estimation: Theory and Application*. Prentice Hall, Mar. 1999.

[26] Y. S. Park, M. H. Cho, C. S. Oh, and Y. J. Kang, "Coherence-based sensor set expansion for optimal sensor placement in active road noise control," *Mechanical Systems and Signal Processing*, vol. 169, p. 108788, 2022. [Online]. Available: https://www.sciencedirect.com/science/article/pii/S0888327021011006

[27] A. Thompson and B. N. Taylor, *Guide for the Use of the International System of Units (SI)*. National Institute of Standard and Technology, Special Pubblication 811, 2008.

[28] G. Cerrato, "Automotive sound quality: Powertrain, road and wind noise," *Sound and Vibration*, vol. 43, pp. 16–24, April 2009.
[29] A. Costalunga, C. Tripodi, L. Ebri, M. Vizzaccaro, L. Cattani, E. Ugolotti and T. Nili, "Experimental results on active road noise cancellation in car interior," in *in Proc. Audio Engineering Society Convention 144*, Milan, May 2018.

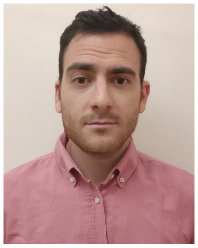

Alessandro Opinto was born in Catania, Italy, in 1991. He received the MSc in Communication Engineering from University of Parma in 2018 and the PhD in Automotive for Intelligent Mobility in 2022 from the University of Bologna. During the 2017, in collaboration with CentraleSupélec University, he was intern at the Mathematical and Algorithmic Sciences Lab of Huawei in Paris, France. Since February 2022 he has been working in R&D department of Keysight Technologies as software and algorithm developer on 5G physical layer. His research interests range from signal processing for Active Noise Control systems to 5G communications.

Marco Martalò (Senior Member, IEEE) received the Ph.D. degree in information technologies from the University of Parma, Parma, Italy, in 2009. From 2012 to 2017, he was an Assistant Professor with E-Campus University, Italy, and also a Research Associate with the University of Parma, Italy, until 2020. Since 2020, he has been an Associate Professor of telecommunications with the University of Cagliari, Italy, where he is part of the Networks for Humans (Net4U) laboratory. He has coauthored the book Sensor Networks with IEEE 802.15.4 Systems: Distributed Processing, MAC, and Connectivity. His research interests are in the design of communication, and signal processing algorithms for wireless systems and networks.

Alessandro Costalunga received the Master Degree in Computer Engineering and the Ph.D. in Information Technology from the University of Parma, in 2013 and 2017, respectively. In 2017, he joined the R&D department of Ask Industries Spa, where he has been working as core developer of active noise control systems and multi-zone audio reproduction systems for the automotive industry.

Nicolò Strozzi was born in Reggio Emilia, Italy, in 1988. He studied Telecommunication Engineering at the University of Parma, Italy, where he obtained his MSc in 2015 and PhD in Information Technologies in 2019. Since February 2019 he has been working in ASK Industries Spa as algorithm designer. His major research fields include localization technologies, audio signal processing, V2X and 5G communications.

Carlo Tripodi (M'12) received the Ph.D. degree in Information Technology in 2016 from the University of Parma (Italy). He was associate researcher in the same institute, working on adaptive signal processing and information theory until March 2017, when he joined the R&D department of ASK Industries Spa. Here he was core developer of Active Noise Cancellation algorithms for the automotive industry. Since 2020 he is responsible for the management of innovative audio projects for automotive systems.

Riccardo Raheli is a Professor of Communication Engineering at the University of Parma, Italy, which he joined in 1991. From 1988 to 1991, he was with the Scuola Superiore S. Anna, Pisa, From 1986 to 1988 he was with Siemens Telecomunicazioni, Milan. In 1990 and 1993, he was a Visiting Assistant Professor at the University of Southern California, Los Angeles, USA. His scientific interests are in the area of systems for communication, processing and storage of information, in which he has published extensively. He has served as Editorial Board Member and Technical Program Committee Co-Chair of prestigious international journals and conferences.